Nanoscale biomemory composed of recombinant azurin on a nanogap electrode

2013 Nanotechnology 24 365301

(http://iopscience.iop.org/0957-4484/24/36/365301)

Nanotechnology **24** (2013) 365301 (8pp) doi:10.1088/0957-4484/24/36/365301

Nanoscale biomemory composed of recombinant azurin on a nanogap electrode

Yong-Ho Chung[1], Taek Lee[1], Hyung Ju Park[2], Wan Soo Yun[3], Junhong Min[4] and Jeong-Woo Choi[1]

[1] Department of Chemical and Biomolecular Engineering, Sogang University, Seoul 121-742, Korea
[2] BT Convergence Division, Electronics and Telecommunications Research Institute (ETRI), Daejeon 305-700, Korea
[3] Department of Chemistry, Sungkyunkwan University (SKKU), Suwon 440-746, Korea
[4] School of Integrative Engineering, Chung-Ang University, Seoul, 156-756, Korea

E-mail: jwchoi@sogang.ac.kr

Received 15 February 2013, in final form 2 July 2013
Published 13 August 2013
Online at stacks.iop.org/Nano/24/365301

Abstract
We fabricate a nanoscale biomemory device composed of recombinant azurin on nanogap electrodes. For this, size-controllable nanogap electrodes are fabricated by photolithography, electron beam lithography, and surface catalyzed chemical deposition. Moreover, we investigate the effect of gap distance to optimize the size of electrodes for a biomemory device and explore the mechanism of electron transfer from immobilized protein to a nanogap counter-electrode. As the distance of the nanogap electrode is decreased in the nanoscale, the absolute current intensity decreases according to the distance decrement between the electrodes due to direct electron transfer, in contrast with the diffusion phenomenon of a micro-electrode. The biomemory function is achieved on the optimized nanogap electrode. These results demonstrate that the fabricated nanodevice composed of a nanogap electrode and biomaterials provides various advantages such as quantitative control of signals and exclusion of environmental effects such as noise. The proposed bioelectronics device, which could be mass-produced easily, could be applied to construct a nanoscale bioelectronics system composed of a single biomolecule.

S Online supplementary data available from stacks.iop.org/Nano/24/365301/mmedia

(Some figures may appear in colour only in the online journal)

1. Introduction

Bioelectronic devices have been researched within the last decade due to their promising potential, which means that they can substitute conventional devices [1–3]. The advance of this technology originated from the development of control of biomolecules and immobilization methods such as the self-assembly process [4–6]. In particular, as active elements, electron transfer proteins provide various advantages for the fabrication of bioelectronic devices owing to their size, structure, and functionality. Metalloproteins play an important role in energy and substance transfer in biological systems, and these reactions are very specific and more effective than other non-biological reactions. The redox state of a metalloprotein can be reversibly changed by reduction and oxidation, and this redox property can be applied to the functions of conventional electronic devices; the signals of these electron transfer proteins can be easily monitored by electrical and electrochemical methods [7, 8].

We are currently focusing on a bioelectronic device containing metalloproteins which could show memory functions by biomechanisms, and several biomemory devices of various types and functions have been developed in our previous research such as multilevel, multifunctional 4-bit biomemory devices [9–11]. These devices have been developed by a combination of biomolecule functions and

silicon-based electronic domains. Metal ions in the center of metalloproteins operate biological functions by reduction and oxidation, and the fundamental concept of a biomemory device is based on this ionic change of metal ions, in which by applying potential reduced and oxidized states of ions can substitute the functions of writing and erasing in a conventional biomemory device.

However, these studies have significant challenges resulting from the properties of biomolecules. Firstly, it is very difficult to control the arrangement of each protein molecule on the solid substrate and to analyze its properties for application to an electronic device due to the fact that the size of a biomolecule is nanometer scale. Secondly, the key function of such proteins is performed in the environment of a solution. Some hindrances caused by the surroundings, such as ions of the electrolyte and a distance effect, occur in the process of electron transfer because the electrical and electrochemical signals of the biomaterials pass through the solution. However, the conditions of high vacuum and extremely low temperature used in the studies of organic or inorganic materials could exclude the effects of surroundings.

For this reason, studies on the application of biomaterials to electronic devices need a new approach. Recently, due to the development of nano-fabrication technology [12–15], the properties of nano-sized functional materials such as CNTs, graphene and biomaterials have been researched by various research groups [16, 17], and these nanoscale devices can also offer a new method for precisely validating the properties of a metalloprotein [18]. However, these nanoscale devices have some limitations with respect to the manufacture of a practical bioelectronics device: (1) electrical stability as an electrode is not guaranteed owing to the problems of the metal–metal junction and pattern uniformity, (2) the signal of each nano-pattern is difficult to control, and (3) mass production of electrodes that have the same electrical properties is impossible.

To overcome these problems, we introduced a nanogap electrode to a previous biomemory device. This approach using a nanogap electrode provides important benefits. It can offer a platform to analyze and control the amount of biomaterial actually utilized in the electrochemical reaction without the effect of signal interference. Nanogap electrodes can be mass-produced reliably because they are fabricated by using well-established lithographic techniques, and thus these nanoscale devices could be utilized not only in the research field but also as practical bioelectronics devices. However, bioelectronic devices using metalloprotein and a nanogap electrode have not been reported yet in spite of these advantages.

In this study, we fabricated nanobiomemory devices composed of recombinant azurin on nanogap electrodes. The size-controllable nanogap electrodes were fabricated by photolithography, e-beam lithography, and surface catalyzed chemical deposition. Cysteine-modified azurin produced by site-directed mutagenesis (SDM) method was utilized as an active metalloprotein, because direct immobilization on a solid surface using the cysteine residue was more stable and effective for biofilm formation. The redox property of recombinant azurin was obtained by cyclic voltammetry (CV) on the nanogap electrodes. We explored the effect of the distance between electrodes for a biomemory device in the nanoscale, and demonstrated memory functions of immobilized metalloprotein using these optimized nanogap electrodes.

2. Experimental details

2.1. Materials

Azurin was modified and expressed with its cysteine residue by site-directed mutagenesis (SDM) methods used to produce mutations by changing the codon for Lys92Cys (K92C) from AAG to TGC. The azurin gene containing plasmids were transformed into *E. coli* BL21 (DE3). The transformed cells were grown for an additional 12 h at 35 °C and were harvested by centrifugation at 4000*g* for 20 min at 4 °C. Recombinant apo-azurin fractions which did not contain copper (elution pH = 4.4–5.0, respectively) were separated on an ion exchange column (S-resin) with a pH gradient ranging from 4.0 to 5.0 (50 mM sodium acetate). $CuSO_4$ (0.5 M) was added to the protein solution and taken up by the recombinant apo-azurin. This process was developed by our research team [19]. The recombinant azurin was purified using an Amicon ultracentrifugal filter (MWCO 3k, Millipore, USA). Reagents including HEPES (4-(2-hydroxyethyl)-1-piperazineethanesulfonic acid) and Cu_2SO_4 were purchased from Sigma Aldrich Co (USA).

2.2. Fabrication of the nanogap electrode

The micro-pattern composed of Cr (10 nm) as an adhesion layer and Au (40 nm) on a Si substrate with thermally oxidized SiO_2 (300 nm) was fabricated by photolithography and an electron beam evaporator. An electron beam lithography system (FEI Sirion 400 FESEM, USA, and Raith Elphy quantum S/W, Germany) was utilized for making nano-patterns. To construct a micro-patterned contact surface, Au was deposited with a thickness of 50 nm. $HAuCl_4$ as a source of gold ions and NH_2OH as a reductant were utilized in the process of surface catalyzed chemical deposition. The normal conditions used for gap narrowing were 64 μM NH_2OH, 27 °C, stirring speed of 1200 rpm, a reaction time of 2 min, and four times. These conditions were sometimes corrected as the occasion demanded.

2.3. Immobilization of protein on the micro- and nano-electrodes

The prepared electrodes were cleaned with piranha solution consisting of 15 vol% H_2O_2 (Duksan Pure Chemical Co. Ltd, Korea) and 85 vol% H_2SO_4 (Daejung Chemical Co. Ltd, Korea) at 70 °C for 10 min to remove contaminants and residues. The electrodes were then rinsed with acetone, isopropyl alcohol, and deionized water sequentially. The modification of the electrodes was carried out by covalent bonding between the thiol group of cysteine and the gold

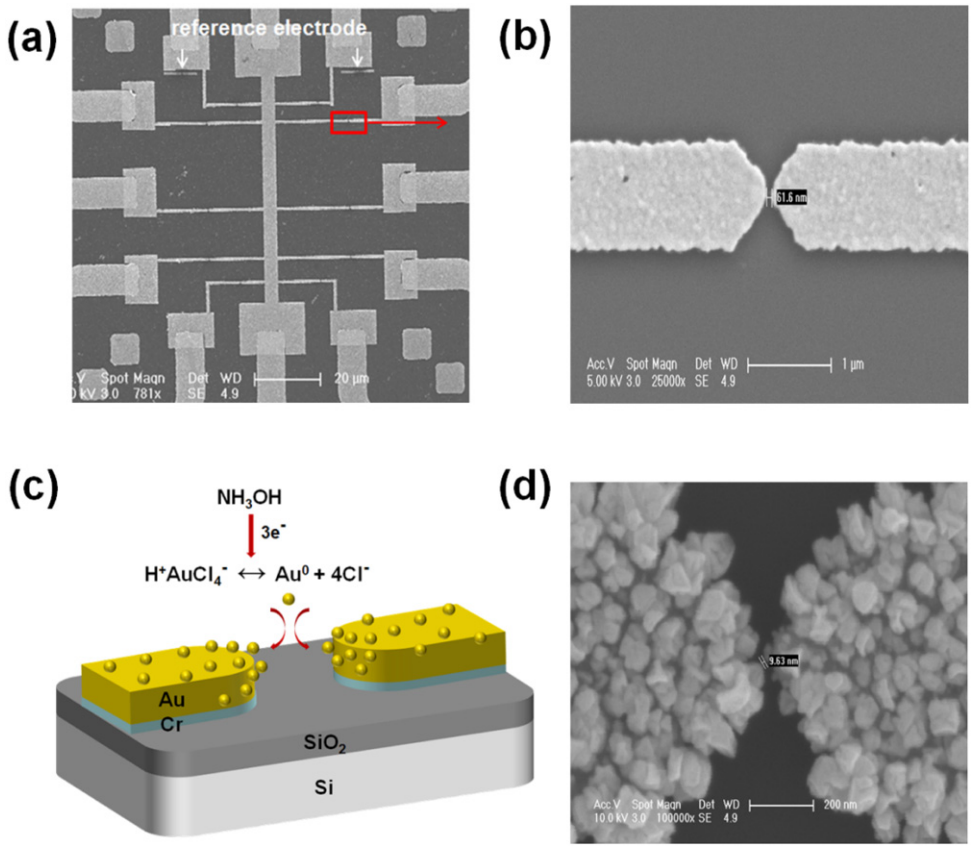

Figure 1. Images of fabricated nanogap electrodes. (a) Overall FESEM image of an electrode patterned by e-beam lithography. The white arrow indicates reference electrodes. (b) Enlarged FESEM image of an electrode patterned by e-beam lithography. (c) Description of the surface catalyzed chemical deposition: reduced gold ions by reductant were deposited on the gold surface. (d) FESEM image of a fabricated nanogap electrode by surface catalyzed chemical deposition (about 10 nm).

surface. The recombinant azurin was dissolved in 10 mM HEPES buffer (pH 7.0) at a concentration of 0.1 mg ml^{-1}. The fabricated electrodes were immersed in protein solution for 3 h at 5 °C, and then washed with DI water and dried under pure N_2 gas.

2.4. Instrumentation

The images of the electrodes were monitored via FESEM (FEI Sirion 400 FESEM, USA) to measure the accurate distance between electrodes, the surface morphology was confirmed by AFM (Digital Instruments Multimode, USA), and the electrical properties of the fabricated nanogap electrodes were measured with a probe station and a semiconductor device analyzer (Agilent B1500A, USA). Those measurements were performed in solid state (air) to confirm the properties of the fabricated devices indirectly. The electrochemical properties of the immobilized protein were confirmed by the techniques of cyclic voltammetry (CV) and chronoamperometry (CA) using a potentiostat/galvanostat (CHI-660, CH Instruments, Inc., TX, USA). All electrochemical measurements of the recombinant azurin immobilized on the micro- and nanogap gold electrodes were performed in 10 mM HEPES buffer (pH 7.0) at a scan rate of 30 mV s^{-1}. The potential ranges were 0.5 to −0.2 V and 0.7 to −0.4 V, respectively, due to the differences in peak positions. Specific details of all measurements are given in figure S1 (see the supplementary data available at stacks.iop.org/Nano/24/365301/mmedia).

3. Results and discussion

3.1. Biomemory device fabrication

Micro- and nano-electrodes of various sizes were utilized in this study to confirm the effects of redox peak variation according to the change of distance at the micro- and nanoscale. Figure 1(a) is an overall image of a gold nano-electrode used in this measurement. The line in the center was employed as a common line, and ten lines were located in the left and the right sections. Reference electrodes were inserted during the process of electron beam lithography to indirectly confirm the changes in gap size, and prevent substrate damage and carbonization of the electrode's surface, except during initial setup of the manufacturing process. It is difficult to confirm protein immobilization on a gold surface by using field effect scanning electron microscopy (FESEM) because the biomaterial is very fragile during exposure to an electron beam, and the morphologies of the nanogap electrodes are relatively rough. Therefore, only gap size was confirmed by FESEM after all fabrication

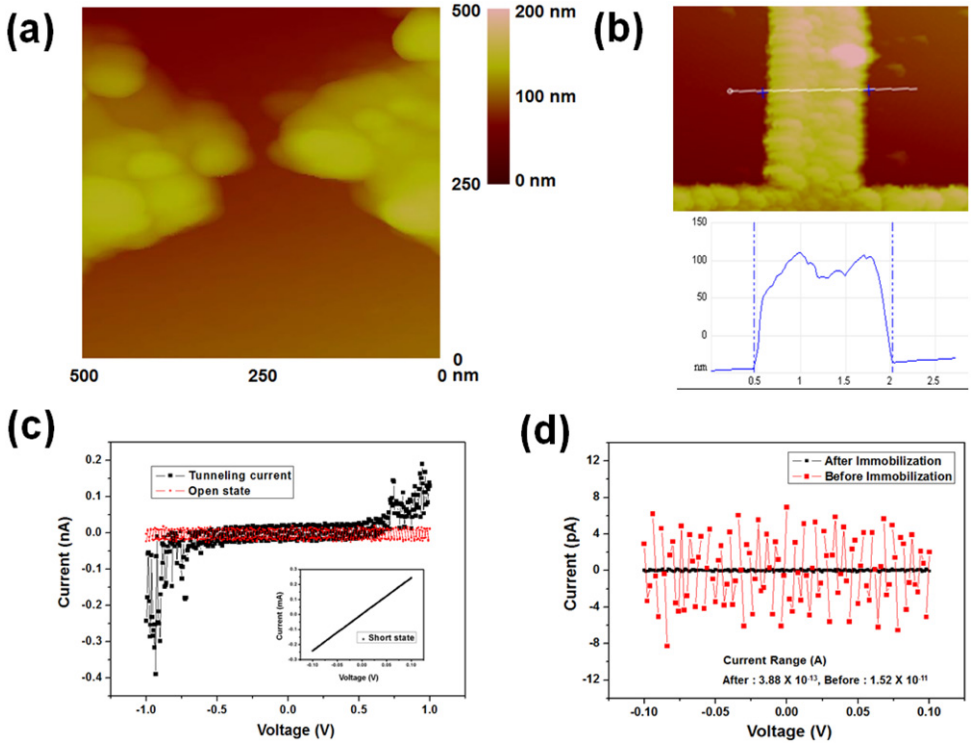

Figure 2. Properties of the fabricated nanogap electrodes. (a) AFM image of a nanogap electrode which has a size of 20 nm. (b) The line profile of the gold pattern resulting from surface catalyzed chemical deposition. (c) The tunneling current was monitored in conditions with an applied voltage of 1 V and the gap size under 1 nm. (Inset: shorted state.) (d) The noise level of two electrodes before and after protein immobilization.

processes and measurements were completed. Figure 1(b) shows electrodes fabricated by electron beam lithography which have an average gap size of 70–80 nm. The variation of gap distance according to the manufacturing process was from 50 to 100 nm. Although the degree of variation was ∼50 nm, nanogap electrodes having relatively uniform sizes could be obtained using a well-established gap narrowing method involving a surface catalyzed chemical deposition process by Yun's group [20], as shown in figure 1(c). The micro-electrodes used for comparison measurements were also fabricated by the same method (see supplementary data figure S2 available at stacks.iop.org/Nano/24/365301/mmedia). The gap narrowing process using the reduction of gold ions was based on the diffusion of gold ions dissolved in the solution. Therefore, the growth ratio gradually decreased as the gap became narrowed because the diffusion could be affected by spatial hindrance due to the decrement of gap distance. A typical nano-electrode (10 nm gap size) fabricated by surface catalyzed chemical deposition is shown in figure 1(d). This gap could be reduced to 1 nm by controlling the process parameters including reductant concentration, temperature and time (see supplementary data figure S3 available at stacks.iop.org/Nano/24/365301/mmedia).

3.2. Properties of the fabricated nanogap electrodes

An atomic force microscopy (AFM) image of a fabricated electrode with a nanogap of ∼20 nm is shown in figure 2(a). The surface formed by the gold ions has irregular polycrystalline patterns, resulting from the method of deposition. This results from the fact that gold ions diffused onto an electrode have a tendency to move toward a more thermodynamically stable globular shape. In addition, growth of the gold electrode mainly occurred on the edge of the pattern, because surface catalyzed chemical deposition is based on the reduction of gold ions by diffusion. Figure 2(b) shows this phenomenon, where the cross section of the electrode has a convex structure on both sides. Electrical shorting of the electrodes might occur during the gap narrowing process. Therefore, the electrical properties of electrodes, as affected by the size of the nanogap, were investigated, as shown in figure 2(c). The current level reached milli-ampere scale (inset) when an electrical short occurred due to attachment of a gold particle fabricated by self-nucleation in the reaction and from unexpected contamination with organic and metallic residues. However, only a pico-ampere scale of current was shown with the successfully fabricated nanogap electrode (red line). A defective electrode could be eliminated using this large current difference. The black line shows the tunneling current between two electrodes which have a gap distance of ∼1 nm. When the applied voltage was ±1 V, a tunneling current of only 0.3 nA was measured and the current could not be measured when a lower voltage and larger gap distance were used. We assumed that the tunneling current can be neglected in the measurement when using an applied voltage under ±1 V and a nanogap electrode >1 nm, as a result of the low amount of generated current. The reasons were that (1) the

redox reaction of immobilized azurin was mainly operated in the potential range between ±0.5 V, and (2) the detection range of the electrochemical measurement was of about a few hundred pico-ampere scale. The current after immobilization of azurin on nanogap electrodes with a gap size of ∼3 nm is shown in figure 2(d). The noise level after immobilization was diminished to fA (black line), whereas its level without protein immobilization was ∼pA (red line). It is likely that environmental noise could be removed due to the fact that the bare electrodes were covered with protein, which plays a role as an insulator at room temperature compared to the metal and organic materials, even though protein is known to be a semiconductor in its solid state [21, 22].

3.3. Electrochemical behavior of recombinant azurin on the micro- and nanogap electrodes

The inset of figure 3(a) represents the electrode structure utilized in this research, in which the working and counter-electrode were patterned oppositely on a flat surface. Because the distance between electrodes in a general electrochemical system is difficult to control precisely, the substrates fabricated with the lithographic technique were used in this experiment. This electrode system was different from the usual system of CV in the aspect of electron transfer between the working and counter-electrodes. Electron transfer in this patterned electrode system was limited by the conical shaped electrode, which resulted in direct transfer between the edges of the two electrodes, whereas electron transfer by a redox reaction was easily accomplished on the bulk electrode because it had a relatively large area and applied the same potential due to the parallel flat electrode structure.

Figures 3(a) and (b) show the cyclic voltammogram of the recombinant azurin molecules with well-defined redox peaks with the reduction potential at E_{pc} and the oxidation potential at E_{pa}, which were generated from the electron transfer process of the recombinant azurin center, $Cu^{2+/1+}$. These redox peaks produced by immobilized azurin were clearly distinguishable from the cyclic voltammogram peaks of the bare nanogap electrode (see supplementary data figure S4(a) available at stacks.iop.org/Nano/24/365301/mmedia). These measurements were taken on microgap electrodes (3 μm–8 μm) and nanogap electrodes (38 nm–1 nm), respectively. Analysis according to the distance in the nanogap electrode was performed in a single electrode which was fabricated with various sizes for precise analysis, because the absolute current level could be dissimilar in each fabricated electrode as a result of the original charge of the metal surface, whereas the difference between fabricated micro-electrodes could be negligible. The aspect of electron transfer due to the redox reaction of the immobilized protein could be varied depending on the distance between the working and counter-electrodes. The common phenomenon of electron transfer in micro- and nano-electrodes was the movement of E_{pc} and E_{pa} in the direction of the standard potential, and this meant that the transfer speed of electrons was increased by diminishing the distance of the pathway. The point of difference was the I_p value which indicated

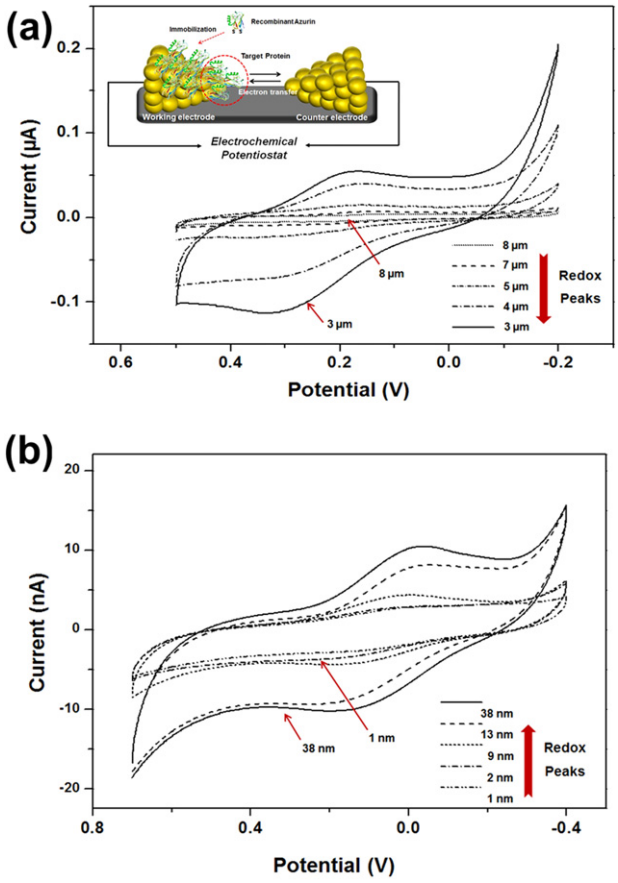

Figure 3. (a) Distance-dependent cyclic voltammogram of recombinant azurin on the microgap electrodes. Inset: overall drawing of the electrode structure utilized in this research. (b) Nanogap electrode.

the absolute amount of current generated from oxidation and reduction of immobilized protein. As shown in figure 3(a), for a micro-electrode, the intensity of the redox peaks was increased by decrement of the gap distance, whereas the opposite phenomenon was observed in the nano-electrodes (figure 3(b)), in which the redox signal was reduced when the gap size was decreased from nearly 38 to 9 nm. It was likely that the number of azurin molecules which could participate in electrochemical reactions was decreased by the narrowed gap.

To explain this difference, we assumed two main pathways of electron movement between two electrodes. The first pathway was a bulk effect produced by diffusion of ions in the electrolyte solution as a general phenomenon in a conventional electrochemical reaction, in which distance was the key factor determining the speed and efficiency of electron movement. The second pathway was the effect of a direct channel being formed in the nearest point of the oppositely patterned electrodes. This direct channel could be explained by resistance differences. Because an immobilized protein on the gold surface has a higher resistance than the bare gold electrode, the electrons induced by an applied voltage move mainly on the gold surface of the working electrode due to the fact that the area contacted with solution is covered with immobilized azurin, and are finally

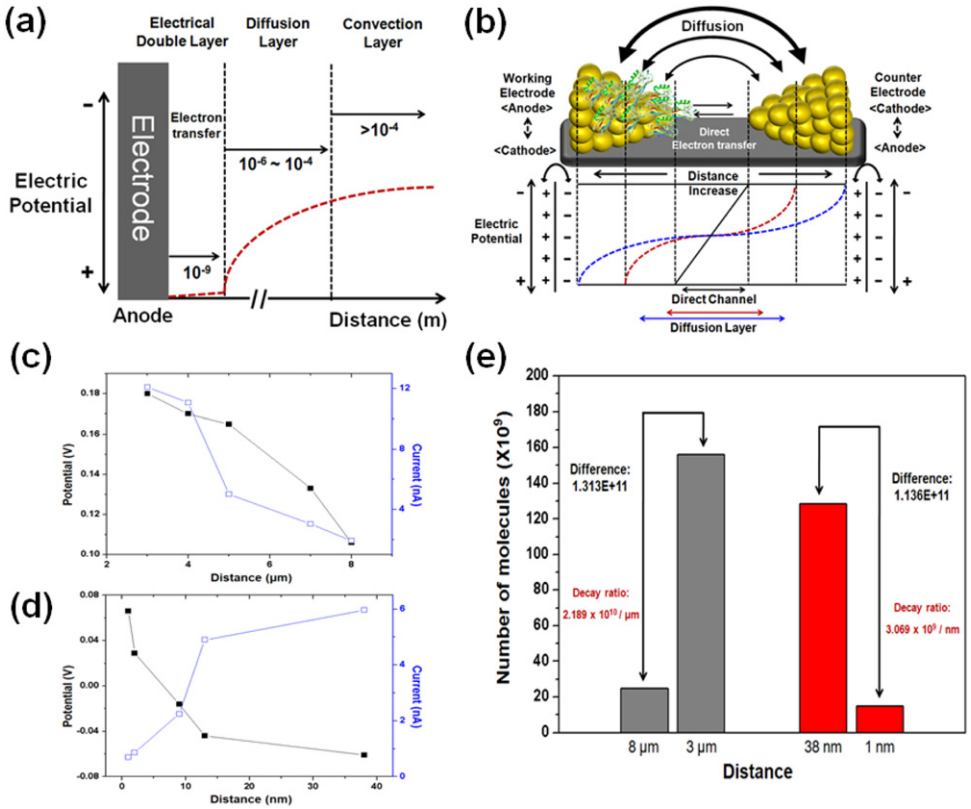

Figure 4. (a) The variation of transfer phase due to the distance from an electrode surface to the other electrode. (b) Two dominant mechanisms of direct channel and diffusion related to electron transfer in the electrolyte solution. The black line, and blue and red dotted lines indicate the potential distribution according to the distance between two electrodes. (c), (d) Quantitative results for E_{pc} and I_p in micro- and nanogap electrodes, respectively. The black and blue lines indicate E_{pc} and I_p, respectively. (e) Comparison of the number of proteins participating in the redox reaction in the cases of the longest and shortest gap distance.

transferred to the counter-electrode at the closest position to the working electrode. The metalloprotein was reduced and oxidized by a specific potential, in which the generated electrons were transferred through passages in the electrolyte. Meanwhile, the total area governed by a specific potential in the substrate could be changed by the shape and distance of the electrodes, based on the variance of electrical field between two electrodes. If the distance between the working and counter-electrode is relatively large, such as the level of a micrometer, the concentrating phenomenon of current transfer is decreased by the bulk effect based on ion diffusion through an electrical field in an electrolyte. In contrast, this phenomenon is reinforced when the distance between the two electrodes becomes smaller, e.g., to the scale of a nanometer. The electrodes utilized in this research had a sharpened shape at their edge, due to their triangular structure. As a result, the quantity of influenced protein immobilized on the electrode by an applied voltage was diminished according to the decrease of the gap size, resulting from diminution of the area related to electron transfer.

3.4. Analysis of electron transfer for the optimization of gap distance

Figure 4(a) shows three kinds of mechanisms related with electron transfer from the surface of an electrode to the other electrode in the electrolyte solution. This phenomenon, related to distance, has been well studied in the field of electrochemistry, though the mechanism has not been precisely defined at the atomic scale [23]. The passages for electron movement in the solution were divided into three regions designated as electrical double, diffusion, and convection layers, in which the area involved in this study ranged from a micrometer to a nanometer. The electrical potential near the electrode surface at the nanoscale level may not be greatly decreased according to the increase in distance from another electrode, because electrons could be transferred directly by an ion channel. It is likely that the ions were arranged sequentially by the strong electrical field and electrons moved through these channels similarly to the movement of holes in a semiconductor. However, when the distance between two electrodes was out of the nanometer level, electron movement was restricted by a drop in potential due to the resistance of the solution, and the diffusion caused by the difference in ion concentrations was the main force to transfer electrons. Figure 4(b) presents a schematic diagram of two mechanisms related to the pathway of electron transfer in this research. The direct channel was formed in the closest area which had a nanoscale distance (black arrow), whereas the diffusion layer produced by the bulk effect was formed at the microscale, in which there were some areas governed

Table 1. The number of molecules related to redox reactions according to the distance between the working and counter-electrodes (Note that the surface coverage was $2.100\,63 \times 10^{-11}$ mol cm^{-2}.)

	Electrode distance	E_{pc}	I_{pc}	Area (cm^2)	Area (μm^2)	Number of molecules
Bulk-scale	~3 mm	0.333	2.453×10^{-7}	2.500×10^{-1}	~5000	3.162×10^{12}
Microscale (μm)	8	0.106	1.925×10^{-9}	1.964×10^{-3}	~443	2.485×10^{10}
	7	0.133	3.039×10^{-9}	3.101×10^{-3}	~557	3.923×10^{10}
	5	0.165	5.012×10^{-9}	5.114×10^{-3}	~715	6.470×10^{10}
	4	0.170	1.106×10^{-8}	1.129×10^{-2}	~1006	1.428×10^{11}
	3	0.180	1.210×10^{-8}	1.235×10^{-2}	~1111	1.562×10^{11}
Nanoscale (nm)	38	−0.061	5.973×10^{-9}	1.016×10^{-2}	~1007	1.285×10^{11}
	13	−0.044	4.900×10^{-9}	8.333×10^{-3}	~913	1.054×10^{11}
	9	−0.016	2.246×10^{-9}	3.820×10^{-3}	~618	4.832×10^{10}
	2	0.029	8.660×10^{-10}	1.473×10^{-3}	~384	1.863×10^{10}
	1	0.066	6.940×10^{-10}	1.180×10^{-3}	~344	1.493×10^{10}

by diffusion, because these were influenced by low electrical fields (red and blue arrows).

Figures 4(c) and (d) show the quantitative results. E_{pc} as the potential of reduction, and I_p as the absolute amount of current are shown by black and blue lines, respectively. The variation of E_{pc} was common for each electrode, in contrast to the different phases of I_p which change as mentioned above. Quantitative analysis was performed using these results to confirm how many proteins participated in each redox reaction. Azurin was initially immobilized on a gold substrate which had a size of 0.25 cm^2 in the conventional arrangement of electrodes at bulk-scale because it could offer reliable results repeatedly (see supplementary data figure S4(b) available at stacks.iop.org/Nano/24/365301/mmedia). The surface coverage was calculated by the following equation [24]:

$$i_p = \frac{n^2F^2\Gamma Av}{4RT} \quad (1)$$

where n is the number of electrons, F is the Faraday constant, Γ is the surface coverage, A is the area in cm^2, ν is the scan rate, R is the gas constant, and T is the temperature (K). The surface coverage and the number of azurin molecules on 0.25 cm^2 of gold substrate were 2.101×10^{-11} mol cm^{-2} and 3.163×10^{12}, respectively. Specific results are shown in table 1. We assumed that this surface coverage of azurin on the bulk electrode was the same as that for micro- and nano-electrodes, although the shape of the electrodes was different. We estimated that the difference in I_p was not based on the amount of immobilized protein on the electrode, but rather the difference of total area influenced by the applied potential. Figure 4(e) shows a quantitative comparison of the number of proteins related to the redox reaction in the cases of the longest and shortest distance. Although the electrode sizes of the micro- and nanogaps have wide differences, such as 8 μm and 0.7 μm in width, respectively, the number of proteins was similar in each case: 3 μm (1.562×10^{11}) and 38 nm (1.285×10^{11}). This result indicated that the direct channel was more effective than the transfer by diffusion. The drop in potential occurred due to a diffusion process resulting from ion disproportion between electrodes, in which the amount of proteins related to the redox reaction was affected by the diminution of area receiving a specific potential.

3.5. Memory functions on the optimized nanogap electrode

The results related to electrochemical measurements in this study can be applied to fabricate a biomemory device similar to that described in our previous study, at bulk-scale [10, 11]. The optimal gap distance for effectiveness was determined to be ~20 nm, because the I_p value converged at that point, whereas it abruptly decreased near 10 nm, as shown in figure 4(d). Using this nanogap electrode, we could demonstrate a memory function consisting of two simple states. A cyclic voltammogram of immobilized azurin utilized in the demonstration of memory functions is presented in figure S5 (see the supplementary data available at stacks.iop.org/Nano/24/365301/mmedia). The oxidation and reduction potentials generated by the redox reaction could be utilized as key parameters to operate a biomemory device. Applying the oxidation potential made it possible to store the positive charge in the recombinant azurin molecules, and this parameter was designated as the 'write' function. Vice versa, applying the reduction potential made it possible to release the positive charge in the recombinant azurin molecules, and this parameter was designated as the 'erase' function. To reliably store and erase the positive charge in the recombinant azurin molecules, two conditions were required: (1) the ability to eliminate and control potentials for the continuous application of the potentials, and (2) a method of minimizing the charging current. These problems could be solved by using a technique called chronoamperometry (CA). The specific mechanism of the biomemory device employed in this research is described in figures S7 and S8 (see the supplementary data available at stacks.iop.org/Nano/24/365301/mmedia). Figure 5 displays a memory function using CA. Here, with respect to the measurement of currents, application of the oxidation voltage is the writing step, whereas application of the reduction voltage is the erasing step. Faradaic currents were observed when the oxidation potential was applied to the fabricated electrode and the azurin molecule became oxidized. At that time, the electrode was left open for a short time period, and again when connecting the reduction potential;

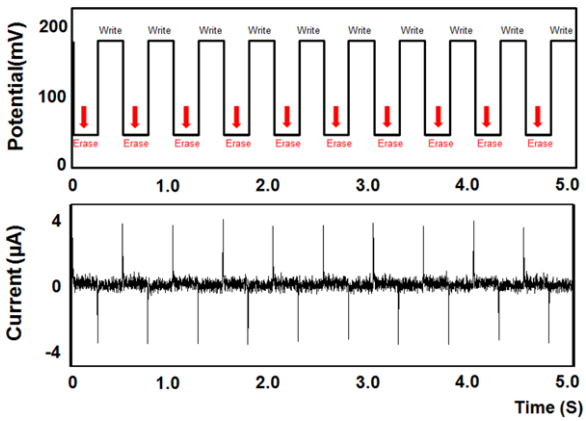

Figure 5. The confirmation of memory functions by CA. The oxidation and reduction potentials were sequentially applied to the nanogap electrode which had a size of 20 nm with a duration of 250 ms.

large amplitude currents were monitored in the absence of background currents; then the stored charge was erased. Similarly to this, when redox potentials were applied to the protein-immobilized electrode for a duration of 250 ms, clear charging and discharging currents used to write and erase functions were clearly monitored, although a jagged noise current was monitored between the applied oxidation and reduction potentials in comparison with memory functions using a micro-electrode (see supplementary data figure S6 available at stacks.iop.org/Nano/24/365301/mmedia).

These results suggest several advantages for the design of a bioelectronic device composed of a pseudo-single metalloprotein or various biomaterials to provide multiple functions in one device. Such a device could measure the redox peaks of the smallest amount of protein, with the same measuring limitations as an electrochemical system. The speed of electron transfer, which is related to the response time and the memory clock, was improved by the application of a nanogap electrode to the electrochemical system.

4. Conclusions

A nanoscale biomemory device was fabricated by a combination of recombinant protein and nano-fabrication techniques. The characteristics of nanogap electrodes fabricated by lithographic techniques and surface catalyzed chemical deposition were measured, and the optimized size of a nanogap electrode for biomemory was determined as 20 nm by evaluating the redox properties of recombinant azurin on the various sizes of nanogap. A memory function composed of two states such as write- and erase-functions was achieved based on the redox properties of recombinant azurin on the optimized nanogap electrode. In our results, the direct channel in the nanogap produced by concentration of an electrical field provided precise and selective measurement of immobilized biomaterials at the edge of an electrode because redox reactions of the metalloprotein on the working electrode were mainly performed at nearby positions to the counter-electrode due to the resistance difference, resulting in exclusion of surrounding effects which could be induced by the electrolyte. The proposed nanoscale biodevice should offer a means to access single biomolecular electronic devices since the development of a bioelectronic device composed of a single molecule still has some challenges to overcome, such as the detection limit for an electrical signal in solution, and the manufacture of a practical bioelectronics device as a reliable platform that can be mass-produced by a conventional method.

Acknowledgments

This research was supported by the National Research Foundation of Korea (NRF) grant funded by the Ministry of Science, ICT & Future Planning (2005-2001333), by the National Research Foundation of Korea (NRF) grant funded by the Korea government (MSIP) (2009-0080860), and by a National Research Foundation of Korea (NRF) grant funded by the Korea government (MEST) (2012K2A2A4021554).

References

[1] Maruccio G *et al* 2005 *Adv. Mater.* **17** 816–22
[2] Mentovich E D, Belgorodsky B, Kalifa I, Cohen H and Richter S 2009 *Nano Lett.* **9** 1296–300
[3] Sorgenfrei S, Chiu C-Y, Gonzalez R L Jr, Yu Y-J, Kim P, Nuckolls C and Shepard K L 2011 *Nature Nanotechnol.* **6** 126–32
[4] Choi J-W and Fujihara M 2004 *Appl. Phys. Lett.* **84** 2187–9
[5] Choi Y-B, Kim H G, Han G H, Kim H-H and Kim S W 2011 *Biotechnol. Bioprocess Eng.* **16** 631–7
[6] Kim M J, Zheng S, Kim T S and Kim S K 2011 *Biochip J.* **5** 39–46
[7] Chung Y-H, Lee T, Min J and Choi J-W 2011 *Colloids Surf.* B **87** 36–41
[8] Kim S-U, Lee T, Lee J-H, Yagati A K, Min J and Choi J-W 2009 *Ultramicroscopy* **109** 974–9
[9] Choi J-W, Oh B-K, Min J and Kim Y J 2007 *Appl. Phys. Lett.* **91** 263902
[10] Lee T, Kim S-U, Min J and Choi J-W 2010 *Adv. Mater.* **22** 510–4
[11] Lee T, Min J, Kim S-U and Choi J-W 2011 *Biomaterials* **32** 3815–21
[12] Bonifas A P and McCreery R L 2010 *Nature Nanotechnol.* **5** 612–7
[13] Bouzehouane K, Fusil S, Bibes M, Carrey J, Blon T, Du M L, Seneor P, Cros V and Vila L 2003 *Nano Lett.* **3** 1599–602
[14] Choi J-W, Nam Y S and Fujahira M 2004 *Biotechnol. Bioprocess Eng.* **9** 76–85
[15] Guo X F *et al* 2006 *Science* **311** 356–9
[16] Cao Q and Rogers J 2009 *Adv. Mater.* **21** 29–53
[17] Geim A K 2009 *Science* **324** 1530–4
[18] Cai D *et al* 2010 *Nature Nanotechnol.* **5** 597–601
[19] Kim S-U, Lee J-H, Lee T, Min J and Choi J-W 2010 *J. Nanosci. Nanotechnol.* **10** 3241–5
[20] Ah C S, Yun Y J, Lee J S, Park H J, Ha D H and Yun W S 2006 *Appl. Phys. Lett.* **88** 133116
[21] Wong K and Mann S 1996 *Adv. Mater.* **8** 928–32
[22] Xu D, Watt G D, Harb J N and Davis R C 2005 *Nano Lett.* **5** 571–7
[23] Armstrong F A and Wilson G S 2000 *Electrochim. Acta* **45** 2623–45
[24] Laviron E 1979 *J. Electroanal. Chem.* **100** 263–70